# Continuous measurements of atmospheric water vapour isotopes in western Siberia (Kourovka)

**V. Bastrikov[1,2,3], H. C. Steen-Larsen[2], V. Masson-Delmotte[2], K. Gribanov[1], O. Cattani[2], J. Jouzel[2], and V. Zakharov[1]**

[1]Ural Federal University, Ekaterinburg, 620002, Russia
[2]LSCE/IPSL, UMR8212, CEA-CNRS-UVSQ, CEA Saclay, Gif-sur-Yvette, 91191, France
[3]Institute of Industrial Ecology UB RAS, Ekaterinburg, 620219, Russia

*Correspondence to:* V. Bastrikov (v.bastrikov@gmail.com)

**Abstract.** The isotopic composition of atmospheric water vapour at the land surface has been continuously monitored at the Kourovka astronomical observatory in western Siberia (57.037° N, 59.547° E; 300 m a.s.l.) since April 2012. These measurements provide the first record of $\delta$D, $\delta^{18}$O and d-excess in this region. Air was sampled at 8 m height within a forest clearing. Measurements were made with a wavelength-scanned cavity ring-down spectroscopy analyzer (Picarro L2130-i). Specific improvements of the measurement system and calibration protocol have been made to ensure reliable measurements at low humidity during winter. The isotopic measurements conducted till August 2013 exhibit a clear seasonal cycle with maximum $\delta$D and $\delta^{18}$O values in summer and minimum values in winter. In addition, considerable synoptic timescale variability of isotopic composition was observed with typical variations of 50–100 ‰ for $\delta$D, 10–15 ‰ for $\delta^{18}$O and 2–8 ‰ for d-excess. The strong correlations between $\delta$D and local meteorological parameters (logarithm of humidity and temperature) are explored, with a lack of dependency in summer that points to the importance of continental recycling and local evapotranspiration. The overall correlation between $\delta$D and temperature is associated with a slope of 3 ‰ °C$^{-1}$. Large d-excess diurnal variability was observed during summer with up to 30 ‰ decrease during the night and the minima manifested shortly after sunrise. Two dominant diurnal cycle patterns for d-excess differing by the magnitude of the d-excess decrease (21 ‰ and 7 ‰) and associated patterns for meteorological observations have been determined. The total uncertainty of the isotopic measurements was quantified as 1.4–11.2 ‰ for $\delta$D, 0.23–1.84 ‰ for $\delta^{18}$O and 2.3–18.5 ‰ for d-excess depending on the humidity.

## 1 Introduction

The isotopic composition of atmospheric water vapour is a valuable source of information for quantifying the processes controlling the hydrological cycle. The saturation vapour pressures and air diffusivities of the natural stable isotopologues of water, $H_2^{16}O$, $HD^{16}O$ and $H_2^{18}O$, are slightly different (Merlivat and Nief, 1967; Majoube, 1971; Merlivat, 1978; Barkan and Luz, 2007; Ellehoj et al., 2013). As a result, fractionation takes place during each phase change such as evaporation from the sea surface (Craig and Gordon, 1965; Merlivat and Jouzel, 1979), soil evaporation and plant transpiration from land surface (Farquhar et al., 2007), condensation in the clouds (Jouzel, 1986; Ciais and Jouzel, 1994), and rain re-evaporation and diffusive exchange processes between raindrop and vapour (Stewart, 1975; Field et al., 2010). This fractionation therefore leads to spatial and temporal variations in the isotopic composition of atmospheric water vapour and precipitation. Thus, stable isotopes of water can be exploited as natural tracers of atmospheric transport patterns and physical processes involving water vapour in the atmosphere.

For the last several decades water isotope measurements have focused on liquid water (precipitation, surface water, soil moisture, etc.) as a means to investigate the hydrological cycle processes (Dansgaard, 1964; Rozanski et al., 1993; Gat, 1996). Fewer measurements of atmospheric water vapour have been made as they have previously required laborious techniques such as cryogenic sampling and subsequent isotope-ratio mass spectrometric (IRMS) analysis (Jacob and Sonntag, 1991; Han et al., 2006; Strong et al., 2007; Uemura et al., 2008).

Recently, new types of infrared laser spectrometers (Kerstel et al., 1999; Crosson et al., 2002; Baer et al., 2002) have been developed, and commercial measurement systems based on wavelength-scanned cavity ring-down spectroscopy (WS-CRDS, Picarro, www.picarro.com) and off-axis integrated cavity output spectroscopy (OA-ICOS, Los Gatos Research, www.lgrinc.com) are available. These instruments perform in situ high-frequency measurements of water vapour isotopic composition with an accuracy similar to that obtained by mass spectrometers (Gupta et al., 2009; Sturm and Knohl, 2010). Kerstel and Gianfrani (2008) have recently reviewed the recent advances in laser-based isotope-ratio measurements. Several intercomparison studies of different instruments have been performed (Aemisegger et al., 2012; Steen-Larsen et al., 2013). However, a range of factors like sensitivity to the level of ambient humidity and instrumental drift have led to the need for an appropriate measurement and calibration protocol (Tremoy et al., 2011; Kurita et al., 2012; Steen-Larsen et al., 2013). This need is particularly critical for measurements made at low humidity levels.

These new infrared laser spectrometers have been successfully deployed in various climates: in the Arctic (Steen-Larsen et al., 2013; Bonne et al., 2014), Europe (Aemisegger et al., 2014), Asia (Wen et al., 2011; Kurita et al., 2013), Africa (Tremoy et al., 2012), and North and South America (Farlin et al., 2013; Berkelhammer et al., 2013; Galewsky et al., 2011). Within the territory of the Russian Federation, so far only precipitation isotopic data have been collected (Kurita et al., 2004) and no long-term water vapour isotope measurements have been published.

Our study is focused on the monitoring station in western Siberia (Kourovka, Russia), providing the first isotopic record of atmospheric water vapour in this region. The work is part of a project investigating the water and carbon cycles in the permafrost and pristine peatlands of western Siberia and their projected changes associated with climate change. In Kourovka we develop a reference site for continuous water isotope observations by different in situ and remote-sensing techniques (Gribanov et al., 2013). The observed isotopic composition variation dynamics at this monitoring site can serve as a good reference for analyzing large-scale West Siberian climate and hydrological cycle variations. The monitoring data are also used to validate and improve atmospheric global circulation models (Butzin et al., 2013; Gryazin et al., 2014) in order to improve the representation of the water isotope variability over the West Siberian area and other regions with similar climate characteristics. This will allow for the production of more accurate and reliable predictions of the water cycle and climate changes in the region of our interest and on the global scale as well.

A water vapour stable isotope analyzer has been installed at Kourovka, together with a meteorological station. Here, we give a detailed overview of the water vapour measurement system and report its changes that allow accurate measurements even at very low winter humidity levels, perform an analysis of the surface water vapour isotopic variations together with a comparison with local meteorological data in order to understand the driving processes behind the variability observed, and report the final calibrated data from one year of continuous monitoring of atmospheric water vapour isotopic composition.

This manuscript is organised in four sections. In Sect. 2, we describe Kourovka site characteristics and field set-up. Section 3 describes the instrument calibration and data processing steps and its results. In Sect. 4, we present the water vapour isotopic data, compare it with local meteorological data and analyse diurnal variability.

## 2 Materials and methods

Throughout this paper, the water vapour isotopic composition is expressed in ‰ using the $\delta$-notation (Craig, 1961). Its definition is based on the equation

$$\delta^* = (R_{\text{sample}}/R_{\text{standard}} - 1) \times 1000 \, [\text{‰}], \tag{1}$$

where $\delta^*$ represents either $\delta D$ or $\delta^{18}O$ and $R$ is the ratio of one of the two stable water isotopes $^1H^2H^{16}O$ or $^1H_2^{18}O$ compared to $^1H_2^{16}O$. The $\delta$-values are normalised vs. the IAEA VSMOW-SLAP scale (IAEA, 2012), which correspond to a two point calibration with a standard defining the scale zero (VSMOW, Vienna standard mean ocean water; Gonfiantini, 1978) and a second reference point (SLAP, standard light Atlantic precipitation).

The second order parameter deuterium excess (hereafter noted as d-excess) is defined as the deviation from the linear relationship observed between $HD^{16}O$ and $H_2^{18}O$ in meteoric waters having a global mean slope of 8 (Dansgaard, 1964; Craig and Gordon, 1965):

$$\text{d-excess} = \delta D - 8 \times \delta^{18}O. \tag{2}$$

### 2.1 Kourovka site characteristics

The atmospheric monitoring station of Kourovka was established in 2009 at the Kourovka astronomical observatory (Fig. 1), which was founded in 1965 as part of the Ural Federal University (the former Ural State University). It is located close to the western boundary of western Siberia (57.037° N, 59.547° E; 300 m a.s.l.), it is surrounded by pristine peatland, and is far from any large city (∼ 70 km from Ekaterinburg). There is no industry or any industrial discharge nearby. The observatory is situated in a clearing 100 m × 100 m, within dense pine forest with an approximate height of 15 m. Local climate is continental. Based on published data for the region, over the past half-century the monthly mean temperatures range from −16 °C (January) to +17 °C (July) with ∼ 460 mm of annual precipitation, peaking in summer (Shalaumova et al., 2010). The site is located ∼ 500 km to the south of the permafrost zone. The observatory infrastructure provides all the means needed to keep a
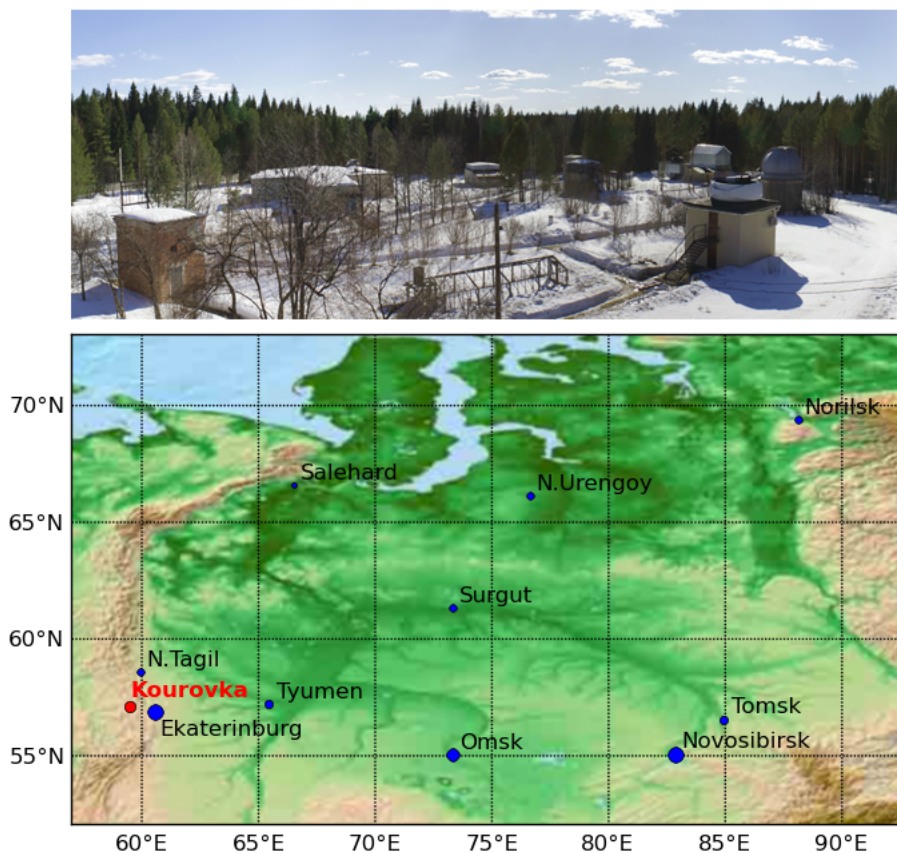
**Figure 1.** Top to bottom: view of Kourovka astronomical observatory, map of western Siberia (from the Ural Mountains on the west to the river Yenisei on the east) showing the location of major cities (blue circles) and the observatory (red circle).

constant year round temperature regime at the device area, non-interruptive power supply and protection from vandalism.

## 2.2 Meteorological data

Since July 2012, a meteorological station MetPak-II (Gill Instruments Ltd., Lymington, UK) has provided high-frequency (1 Hz) continuous measurement of the following atmospheric variables: barometric pressure ($\pm 0.05$ kPa), relative humidity ($\pm 0.8$ % at 23 °C), air temperature ($\pm 0.1$ °C), wind speed ($\pm 2$ % at 12 m s$^{-1}$), wind direction ($\pm 3°$ at 12 m s$^{-1}$) and dew point temperature ($\pm 0.15$ °C). These data are used to compare the humidity measurements performed by the isotope analyzer with meteorological measurements and to investigate the relationships between water vapour isotopic composition at the surface and local meteorological data (see Sects. 4.2 and 4.3).

## 2.3 Isotopic measurement set-up

Water vapour isotopic composition is measured with the laser spectroscopy analyzer L2130-i (Picarro Inc., Sunnyvale, CA, USA) based on WS-CRDS (Brand et al., 2009; Crosson et al.,

2002). The instrument was installed in Kourovka in mid-March 2012 and has been providing high-frequency ($\sim$ 1 Hz) continuous measurements of $\delta$D and $\delta^{18}$O since April 2012.

The analyzer is installed in an air conditioned room (temperature $18 \pm 1$ °C). A shielded air intake is installed on the roof of the building (8 m a.g.l.) and a heated 6 m inlet line (O'Brien optical quality stainless steel tube, 9.5 mm (3/8 inch) OD) is connected with the analyzer. A 5 L min$^{-1}$ pump ensures quick transport of air through the inlet tube. Electric heat tracing (type HKSI, HORST GmbH, Lorsch, Germany) maintains the temperature of the tube at 55–60 °C over the entire tube length.

The analyzer is programmed to perform self-calibrations after every six hours of ambient air measurement using the automated Picarro standards delivery module (SDM). Each calibration is made with two reference water samples: DW (distilled water, $\delta$D $= -96.4$ ‰, $\delta^{18}$O $= -12.76$ ‰) and YEKA (Antarctic snow and distilled water mix, $\delta$D $= -289.0$ ‰, $\delta^{18}$O $= -36.71$ ‰). Each reference sample is measured continuously for 30 min. A third depleted reference sample DOMEC (water standard from Laboratoire des Sciences du Climat et de l'Environnement (LSCE), $\delta$D $= -424.1$ ‰, $\delta^{18}$O $= -54.05$ ‰) is also used periodically to
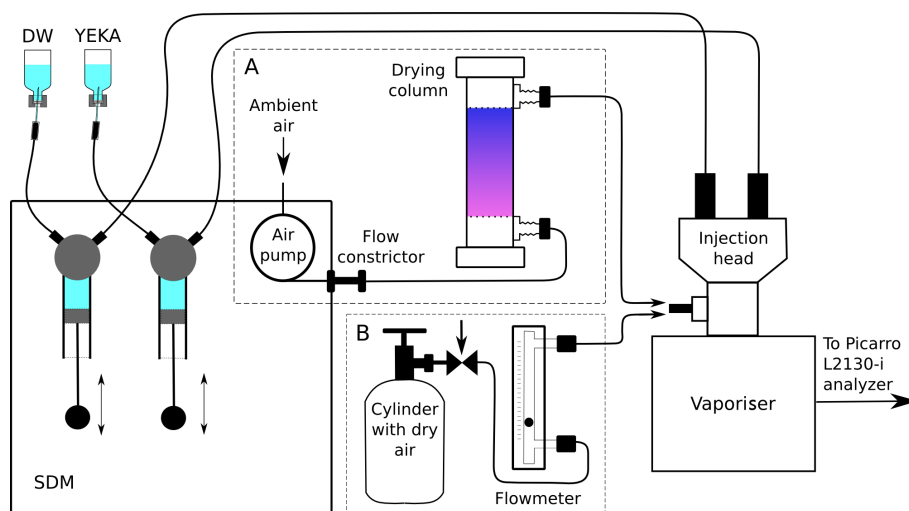
**Figure 2.** Illustration of the set-up used for **(A)** routine calibrations and **(B)** humidity–isotope response calibration.

assess the instrument linearity. The isotopic values of these reference waters in the VSMOW-SLAP scale were measured at LSCE by IRMS with accuracies of 0.5 ‰ for $\delta D$ and 0.05 ‰ for $\delta^{18}O$.

An illustration of our calibration set-up is shown on Fig. 2. The liquid standard is drawn from container by syringe pump of the SDM and transferred via capillary line into the Picarro injection head (C0105) of the Picarro vaporisation module (A0211) which is set at 140 °C. Evaporated standard is then mixed with dried room air pumped at a rate of 12 L h$^{-1}$ through a 450 cm$^3$ drying column filled with DRIERITE desiccant (supplier no. 23001, W. A. Hammond Drierite Company, Ltd., USA, www.drierite.com). The change of the desiccant colour from blue to pink indicates when its activity is depleted. Finally, the mixed standard water vapour is supplied into the Picarro analyzer. Adjustment of the reference water injection speed (between 0.002 μL s$^{-1}$ and 0.08 μL s$^{-1}$) allows water vapour concentration to be regulated within desired limits (in the range 800–30 000 ppmv). During calibration cycles, the humidity is usually set to 12 000 ppmv.

The following technical improvements of the standard Picarro configuration have been made:

– Substitution of the flexible metallised bags for reference water standards with 15 mL glass bottles. This allows to visually control the absence of bubbles in the water, absence of condensed water on the walls inside the bottle and remaining amount of the water standard. Condensed water could be easily removed from the walls by simple shaking, if needed. It is also easy to control the dryness of an empty bottle before filling it with the standard. The bottles are refilled to three-fourths of the volume once per week and installed in an upside down position. The water intake needle is introduced in the lower part of the bottle through the hole in the cap.

– Usage of disposable silicon septa inside the bottle caps. This prevents bubble formation during insertion of a needle into the bottle.

– Replacement of ceramic syringe pumps with the newer Picarro glass syringe pumps equipped with the soft plunger sealing (Tecan Systems, Inc., Ball-end 250 μL syringe, Ref. 19931 C X18A). This allows for the avoidance of air bubbling in the sealing between the plunger and syringe walls.

– At the humidity levels below 4000 ppmv, we observe inconsistent calibration results (see Sect. 3.2) and thus substituted the air drying line (Fig. 2a) with the zero air gas supply from a 10 L tank cylinder (Fig. 2b). A calibration gas mixture of N$_2$ + O$_2$ (O$_2$ = 20 % ±1 %) have been used (PGS-Service, Russia, www.pgs.ru) with the following content of impurities: H$_2$ ≤ 0.0001 %, CO$_2$ ≤ 0.0008 %, CO ≤ 0.0004 %, CH$_4$ and other hydrocarbons ≤ 0.0005 %, H$_2$O at normal conditions ≤ 0.0002 %. The guaranteed dew point for the gas equals to −80 °C, which corresponds to approximately 0.5 ppmv of water vapour. For the flow rate control a purgemeter Sho-Rate 1350 with 3–65 Glass Tube (Serv'Instrumentation, France) have been used. The gas flow rate was kept within the range 10–35 L h$^{-1}$.

## 3 Calibration protocol

In order to allow the water vapour measurements comparison with other data, it is important to perform a thorough characterisation of the individual instrumental system response. In this study we follow the calibration protocol described by Steen-Larsen et al. (2013). The major steps of the instrument calibration and data processing are discussed below. Prior to
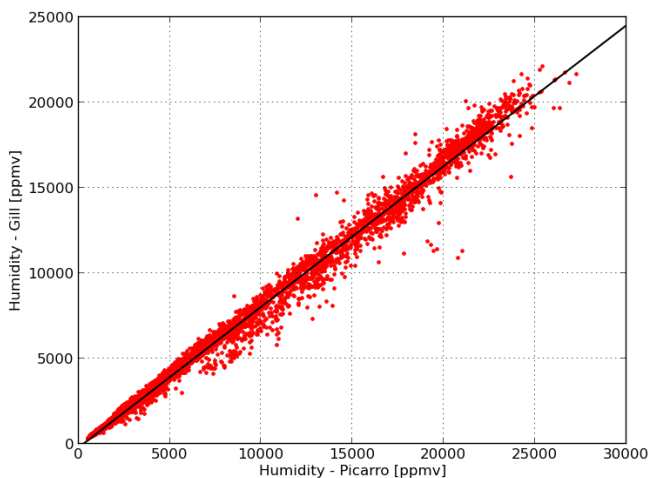
**Figure 3.** Humidity measurements: meteorological sensor (Gill Instruments) vs. Picarro. Black curve: linear fit (Eq. 3).

these steps, we found it useful to perform a quality control of the raw data that includes the search and removal of random instrumental spikes in the data and artefacts due to power supply disturbances or other short-term technical problems.

## 3.1 Humidity correction

Picarro humidity measurements (absolute humidity measured in ppmv) are compared to humidity values calculated from the Gill meteorological measurements (relative humidity and temperature) in Fig. 3. The best fit is given by a linear function ($R^2 = 0.992$):

$$y = -231 + 0.825x, \tag{3}$$

where $x$ is the Picarro and $y$ is the Gill humidity value (in ppmv), respectively. Equation (3) is hereafter used to translate all Picarro humidity data into the meteorological instrument scale.

In other studies, different results of comparing Picarro measurements with independent humidity observations have been reported. Aemisegger et al. (2012) also showed a linear response of the analyzers when comparing to a dew point generator used to control humidity level in the range from 4000 to 31 000 ppmv. Tremoy et al. (2011) (in the range from 5000 to 36 000 ppmv) and Bonne et al. (2013) (in the range from 1000 to 18 000 ppmv) showed a non-linear response of the analysers compared to independent meteorological device observations.

## 3.2 Humidity–isotope response calibration

The humidity–isotope response needs to be determined for each individual instrument, because isotopic measurements are sensitive to absolute water concentration (Steen-Larsen et al., 2013). The cause of this dependence is related to the spectral baseline being dependent on the height of the $H_2^{16}O$

spectral peak. Non-perfect correction in the Picarro software for this influence means that a "manual" on-site characterisation is needed.

The instrument's humidity–isotope response function was determined for the analyzer during its installation and is verified several times a year. This calibration is established by introducing the two water standards (DW and YEKA) at different humidity levels within the whole operational range. Resulting humidity–isotope response functions are shown in Fig. 4 (green – DW standard, blue – YEKA standard). The data are displayed for humidity levels below 5000 ppmv only, as the instrument response appears flat for higher levels. The $y$ axis shows a bias with respect to the mean value measured at 12 000 ppmv. For the standard Picarro calibration set-up we obtained different humidity dependencies for $\delta^{18}O$ measured in different water standards and opposite dependencies for $\delta D$. The most plausible reason for this artefact is incomplete air drying in the DRIERITE column. To confirm this hypothesis, a humidity calibration was performed with a supply of dry gas from a tank cylinder rather than gas passed through the DRIERITE. The exact concentration of $H_2O$ in the filled container was measured as $0.5 \pm 0.1$ ppmv. With this set-up, we obtained, within uncertainty, the same calibration curves for the two standards (red – DW standard, black – YEKA standard, with one conjoint fitting line shown in red). Moreover, the overall humidity dependency became significantly less pronounced for the range 800–5000 ppmv. This indicates the importance of using "dry" air with very limited residual water vapour when performing calibrations at low humidity. Table 1 gives the analytical expressions used to obtain the best fit for the humidity–isotope response function in different cases and the associated coefficients.

Note that there are no data for the DRIERITE experiments below 800 ppmv due to the technical limitations of SDM. The behaviour of the humidity–isotope response functions for these conditions is therefore unknown.

Since all periodical self-calibrations were performed using dry air generated from DRIERITE, we used the humidity–isotope response functions from Eqs. (1)–(4) (Table 1) to correct the reference water sample measurements. To correct the ambient water vapour isotope measurements, we used the humidity–isotope response functions obtained using dry air (Table 1, Eqs. 5–6).

## 3.3 Known-standard calibration

For the period from June 2012 to September 2012, most of the instrument calibrations were invalidated due to a leakage in one of the standards delivery module syringes. The ceramic syringes of the SDM were replaced in September 2012 using a new type of glass syringe; this led to very stable and reproducible calibrations. The data discussed in this paper is therefore limited to the one-year period starting from 21 September 2012. The earlier data starting at the beginning of the instrument's operation is limited to $\delta D$ measurement.
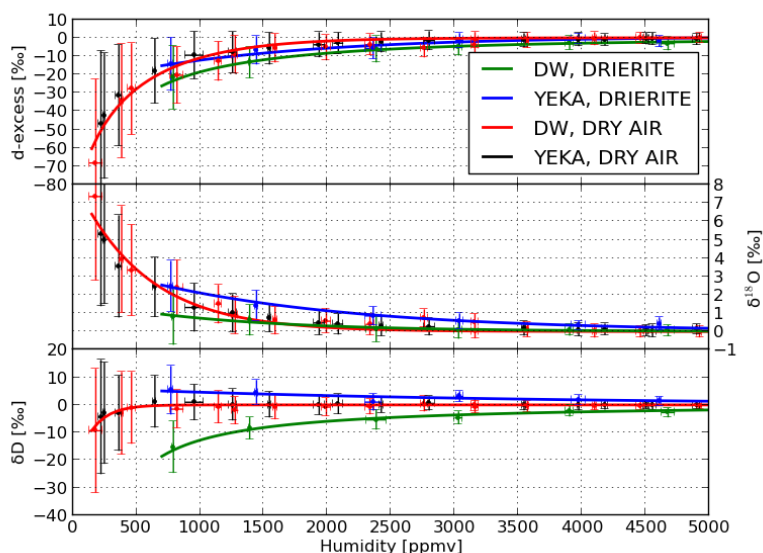
**Figure 4.** Picarro humidity–isotope response functions. Green error bars: calibration performed using DW standard and DRIERITE column, blue error bars: calibration performed using YEKA standard and DRIERITE column, red error bars: calibration performed using DW standard and dry gas, black error bars: calibration performed using YEKA standard and dry gas. Solid lines represent linear fits to the data. For the measurements of DW and YEKA standards using dry air one conjoint fitting line is shown in red. The $y$ axis shows a bias with respect to the mean value measured at 12 000 ppmv.

**Table 1.** Humidity correction functions and coefficients for DW and YEKA standards.

| $N$ | Standard | Isotope | Function | $a$ | $b$ |
|---|---|---|---|---|---|
| 1 | DW | $\delta^{18}O$ | $y = a \cdot \exp(-x/b)$ | $0.952 \pm 0.153$ | $1863 \pm 344$ |
| 2 | (with DRIERITE) | $\delta D$ | $y = a + b/x$ | $0.820 \pm 0.107$ | $-13\,160 \pm 315$ |
| 3 | YEKA | $\delta^{18}O$ | $y = a \cdot \exp(-x/b)$ | $3.770 \pm 0.157$ | $1653 \pm 79$ |
| 4 | (with DRIERITE) | $\delta D$ | $y = a \cdot \exp(-x/b)$ | $6.224 \pm 0.480$ | $3270 \pm 322$ |
| 5 | DW & YEKA | $\delta^{18}O$ | $y = a \cdot \exp(-x/b)$ | $8.394 \pm 0.123$ | $551.0 \pm 11.3$ |
| 6 | (with dry gas) | $\delta D$ | $y = a \cdot \exp(-x/b)$ | $-26.98 \pm 3.80$ | $140.4 \pm 13.2$ |

However, these limited results were compared well with model estimates and FTIR measurements (Gribanov et al., 2013).

During the first two winter months, the humidity level at which calibrations were performed was manually decreased to $\sim 4000$ ppmv in order to reach a level close to the ambient air humidity. However, the instrumental noise induced a loss of accuracy in the calibrations (as reported in Sect. 3.2). We therefore set the humidity level back to $\sim 12\,000$ ppmv.

Figure 5 shows the complete set of calibrations conducted during the period from 21 September 2012 to 31 August 2013 with the VSMOW-SLAP slopes calculated from the measurements. Overall, 1672 calibrations have been made, among which 1552 (93 %) were successful (781 for DW standard and 771 for YEKA standard).

Two-standard calibrations were performed after every six hours of ambient air measurements. For each standard, the averaging window was selected within a steady plateau area,

usually during the last three minutes of the half-hour measurement. After each calibration, the first 13 min of ambient air measurements were discarded to ensure that any calibration water vapour is purged out of the system. The length of these time periods was found to be reasonable for our particular instrument on the basis of the measurement data. We refer the reader to the supplementary material for details.

Standard deviations calculated over the averaging windows range between: 0.4–2.5 ‰ for $\delta D$ (with mean 0.9 ‰), 0.15–0.50 ‰ for $\delta^{18}O$ (with mean 0.25 ‰) and 10–400 ppmv for humidity level (with mean 65 ppmv). Conversion of all humidity-corrected measurements to the VSMOW-SLAP scale upon known reference water samples have been performed at this step, assuming a linear instrumental drift between calibrations and bracketing a given vapour measurement. Overall, the analyzer drift during the one-year period was < 2 ‰ for $\delta D$ and < 0.5 ‰ for $\delta^{18}O$, resulting in
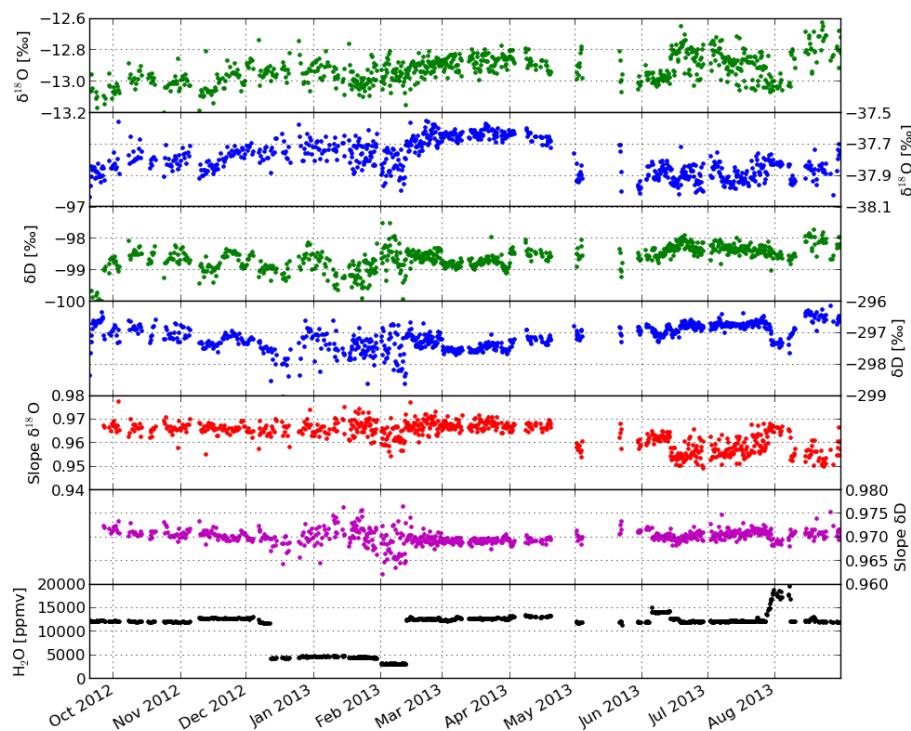
**Figure 5.** Picarro calibration data. Top to bottom: measured $\delta^{18}O$ and $\delta D$ values in ‰ for DW standard (green dots) and YEKA standard (blue dots), calculated calibration slope for $\delta^{18}O$ measurements (red dots) and $\delta D$ measurements (purple dots), humidity concentration in ppmv (black dots).

VSMOW-SLAP slope change $< 0.015$ for $\delta D$ and $< 0.03$ for $\delta^{18}O$.

### 3.4 Total measurement uncertainty

Steen-Larsen et al. (2013) conservatively estimated the instrument precision and accuracy, when calibration was working properly, to be 1.4‰ for $\delta D$, 0.23‰ for $\delta^{18}O$ and 2.3‰ for d-excess at humidity levels between 1500 and 6000 ppmv, respectively. Following Steen-Larsen et al. (2013), we assume that we have similar precision and accuracy at these humidity levels and conservatively decide to use them for higher humidity levels.

At lower humidity levels, we observe an increase of the standard deviation of our measurements (see Fig. 4, red and black error bars) by a factor 4 at 1000 ppmv and a factor 8 at 500 ppmv. We therefore estimate the uncertainty between 1000 and 1500 ppmv to be 5.6‰ for $\delta D$, 0.92‰ for $\delta^{18}O$ and 9.2‰ for d-excess, and between 500 and 1000 ppmv to be 11.2‰ for $\delta D$, 1.84‰ for $\delta^{18}O$ and 18.5‰ for d-excess. Subsequently we decided not to report any measurements for values below 500 ppmv.

Such low humidity levels are encountered at Kourovka during winter. In total, 16 % of all hourly measurements have been made at humidity levels $< 1500$ ppmv (42 % of the winter measurements) and 2.5 % of the measurements have been made at humidity levels $< 500$ ppmv (6.4 % of the winter

measurements). In order to indicate the total uncertainty of the final calibrated data, a specific quality flag has been assigned to each measurement depending on the relevant humidity level.

### 4 Results and discussions

Our Picarro isotopic analyzer has been operated continuously since April 2012 with only occasional short gaps due to electricity interruptions and minor breakdowns. Overall, for the reported period from 21 September 2012 to 31 August 2013, 6794 hourly Picarro measurements have been obtained, which corresponds to 82 % of the total duration (8280 h). The hourly averaged Picarro humidity and isotopic data and Gill meteorological data are presented in Fig. 6, after applying all the corrections and calibrations discussed in the previous section.

Humidity concentration varies from $\sim 250$ ppmv in winter up to $\sim 23\,000$ ppmv in summer, and co-varies with local surface air temperature. The seasonal cycle of $\delta D$ and $\delta^{18}O$ is parallel with the seasonal cycle of humidity and temperature, with the respective ranges of variation being $-103$‰ to $-300$‰ and $-14$‰ to $-39$‰. Maximum values are observed in summer (August), and minimum values in winter (January).
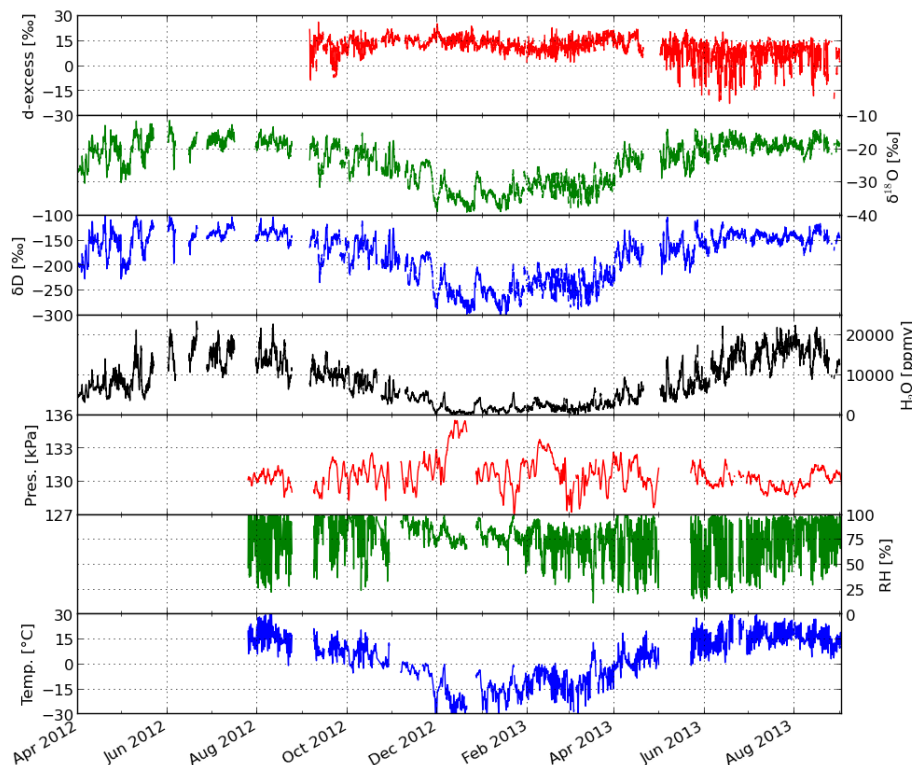
**Figure 6.** Isotopic and meteorological measurements at Kourovka site. Top to bottom: d-excess, $\delta^{18}O$ and $\delta D$ in ‰, humidity concentration in ppmv, pressure in kPa, relative humidity in %, and temperature in °C. Deuterium excess values are not reported before September 2012, due to instabilities of calibrations during this period.

In addition to the seasonal pattern, significant variations are observed on a timescale of several days with respective magnitudes of 3000–8000 ppmv, 50–100 ‰, 10–15 ‰ and 2–8 ‰ in humidity, $\delta D$, $\delta^{18}O$ and d-excess.

Deuterium excess values are only reported after September 2012, due to the instabilities in the calibrations during the first months of measurement. They show a lagged seasonal cycle, with maximum values in winter ($\sim 20$ ‰) and minimum values in summer ($\sim 5$ ‰ during the day and $\sim -25$ ‰ during the night). On a day-to-day basis, deuterium excess variations have a magnitude of less than 3 ‰. Opposite to this, the summer deuterium excess variability is much larger at the diurnal scale; this feature is further investigated in Sect. 4.3.

Our observed seasonal cycles in isotopes are consistent with earlier results obtained from northeast Siberia precipitation data by Kurita (2011). His record showed the peak $\delta^{18}O$ occurring in late summer, and minimum in mid-winter; his d-excess values decrease strongly during summer months, also reaching negative values. However, the maximum d-excess values were observed during mid-autumn and were attributed to increased kinetic effects due to the Artic-origin air mass contribution during this period. Yet this feature does not appear in our 2012 record. Extending the Kourovka record over several years would allow the average seasonal cycle to be established and this contribution to be analysed.

**Table 2.** $\delta D$ vs. $\delta^{18}O$ (linear fit parameters for hourly averaged data).

| Period | $N$ | Slope | Intercept | $R^2$ |
|---|---|---|---|---|
| All data | 6787 | $7.49 \pm 0.01$ | $-1.94 \pm 0.27$ | 0.99 |
| All data (daytime) | 2542 | $7.74 \pm 0.01$ | $6.75 \pm 0.30$ | 0.99 |
| Autumn | 1362 | $7.20 \pm 0.03$ | $-5.78 \pm 0.65$ | 0.98 |
| Winter | 2619 | $7.73 \pm 0.02$ | $4.40 \pm 0.78$ | 0.98 |
| Spring | 1101 | $6.85 \pm 0.05$ | $-14.3 \pm 1.2$ | 0.94 |
| Spring (daytime) | 408 | $7.24 \pm 0.06$ | $-3.55 \pm 1.28$ | 0.98 |
| Summer | 1705 | $5.57 \pm 0.07$ | $-39.6 \pm 1.4$ | 0.76 |
| Summer (daytime) | 634 | $7.02 \pm 0.06$ | $-7.74 \pm 1.22$ | 0.95 |

## 4.1 $\delta D$ vs. $\delta^{18}O$

Figure 7 shows the relationship between surface vapour $\delta D$ and $\delta^{18}O$ through the complete campaign period (left panel) and for each season (right panels). Fitted parameters are presented in Table 2. Here and after, seasons are defined as follows (based on Kourovka climate): 21 September–27 November (Autumn, $N = 1362$), 28 November–31 March (Winter, $N = 2619$), 1 April–31 May (Spring, $N = 1101$) and 1 June–31 August (Summer, $N = 1705$).
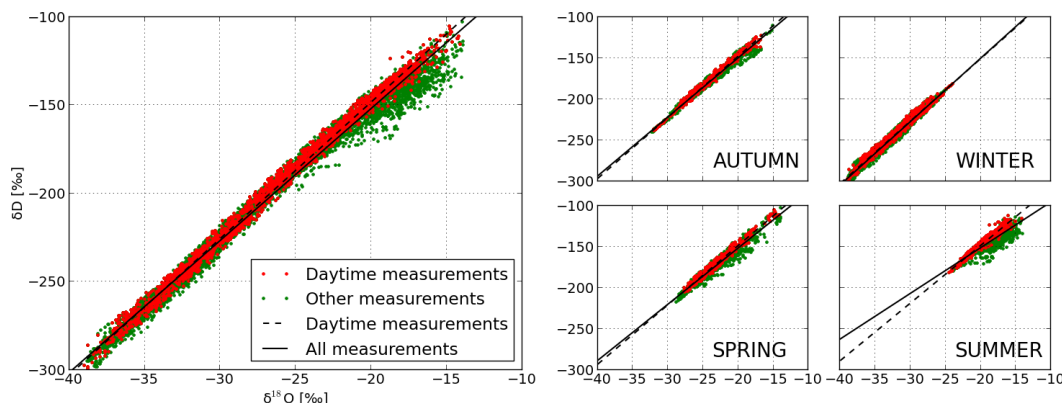
**Figure 7.** $\delta$D vs. $\delta^{18}$O. Left panel: all measurements, right panels: seasonal measurements, red dots: daytime measurements (from 12:00 to 21:00 LT), green dots: all other measurements, dashed line: linear fit through daytime measurements of the graph, solid line: linear fit through all measurements of the graph. See Table 2 for calculations of determination coefficients and slopes.

The linear slope fitted through all the measurements (red and green dots on Fig. 7) equals 7.5 for the whole data set and varies for different seasons from the maximum value (7.7) in winter to the minimum value (5.6) in summer (solid lines on Fig. 7). For all seasons, strong coefficients of determination are observed ($R^2 > 0.94$), with the exception of summer where the coefficient of determination is smaller ($R^2 = 0.76$).

As we observe strong diurnal cycles in the measurements time series, the relationship between $\delta$D and $\delta^{18}$O have been analyzed separately for the daytime measurements. For this we take the measurements performed during the daytime period from 12:00 to 21:00 local time (hereafter LT), which is free from strong variability (red dots on Fig. 7). In this case, we observe significant change of the slopes for spring (from 6.9 to 7.2) and summer (from 5.6 to 7.0) (dashed lines on Fig. 7) with higher coefficients of determination ($R^2 > 0.95$). The overall value of the slope for the daytime measurements equals 7.7.

These results point out the significant role of local processes during the warm seasons in this region indicating a possible influence of continental recycling. During spring and summer, we observe both a loss of correlation and a change in slope, which are caused by the night measurements detachment from the overall strong correlation between $\delta$D and $\delta^{18}$O. The reasons for this effect are discussed in Sect. 4.3.

Our slope values are comparable to the 6.8 value reported by Bonne et al. (2013) for the 1.5 year monitoring data in southern Greenland and the 6.5 value reported by Steen-Larsen et al. (2013) for NW Greenland in summer. In the latter work, separation of high d-excess measurements from the full data set also led to the higher slope values (7.4 for high d-excess measurements and 7.2 for non-high d-excess measurements).

## 4.2 $\delta$D vs. local meteorological data (humidity and temperature)

Figure 8 shows interdependencies of isotopic composition ($\delta$D) and meteorological data (temperature and humidity) for the full data set (left panels) and for each season (right panels) with fitted parameters presented in Table 3.

For $\delta$D, the strongest correlations are observed with the logarithm of humidity, which is consistent with what is expected from Rayleigh distillation. We report $R^2 = 0.88$ for all data, about 0.6 for autumn and winter, and 0.3–0.4 in spring and summer. The slopes are changing from 52 to 26 ‰ per log(humidity [ppmv]); the weakest ones can also be seen to occur in spring and summer.

A strong relationship is also observed between $\delta$D and temperature, as expected from the close relationship between temperature and logarithm of humidity, albeit less strong than the correlation with logarithm of humidity. We report $R^2 = 0.84$ for all data, about 0.6 for autumn and winter and much lower for spring and summer (0.15). The overall relationship has a slope of 3.1 ‰ °C$^{-1}$, with even lower isotope-temperature slopes in spring (1.0 ‰ °C$^{-1}$) and summer (0.9 ‰ °C$^{-1}$).

For Rayleigh distillation, the slope between water vapour and temperature is very close to the slope between precipitation isotopic composition and temperature and equals 0.8 ‰ °C$^{-1}$ for $\delta^{18}$O and 6 ‰ °C$^{-1}$ for $\delta$D. The overall slope value for our observations is about half the relationship expected from Rayleigh distillation. Bonne et al. (2013) have analyzed the relationship between $\delta^{18}$O in vapour and local temperature for southern Greenland and obtained a slope of 0.37 ‰ °C$^{-1}$, which is about half of the value expected from Rayleigh distillation. However, Steen-Larsen et al. (2014) observed the 0.81 ‰ °C$^{-1}$ value for the slope in NW Greenland during summer.
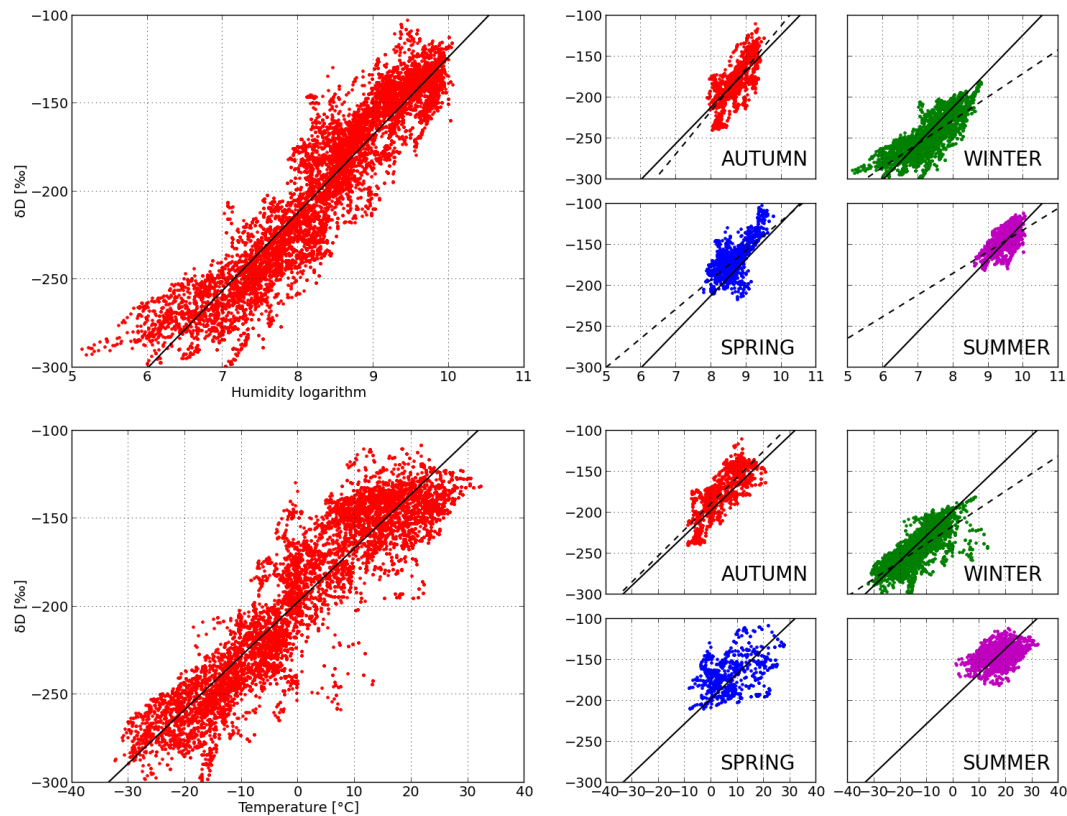
**Figure 8.** $\delta$D vs. logarithm of humidity (top) and $\delta$D vs. temperature (bottom). Left panels: all measurements, right panels: seasonal measurements, solid line: linear fit through all measurements, dashed line: linear fit through seasonal measurements. See Table 3 for calculations of determination coefficients and slopes.

**Table 3.** $\delta$D vs. meteorological data (logarithm of humidity and temperature) (linear fit parameters for hourly averaged data).

| Period | $N$ | $\delta$D vs. logarithm of humidity | | | $\delta$D vs. temperature | | |
|---|---|---|---|---|---|---|---|
| | | Slope | Intercept | $R^2$ | Slope | Intercept | $R^2$ |
| All data | 6787 | $44.3 \pm 0.2$ | $-566 \pm 2$ | 0.88 | $3.06 \pm 0.02$ | $-197 \pm 0.3$ | 0.84 |
| Autumn | 1362 | $52.2 \pm 1.2$ | $-634 \pm 10$ | 0.59 | $3.19 \pm 0.08$ | $-189 \pm 0.6$ | 0.60 |
| Winter | 2619 | $29.7 \pm 0.4$ | $-464 \pm 3$ | 0.65 | $2.23 \pm 0.04$ | $-215 \pm 0.6$ | 0.56 |
| Spring | 1101 | $35.9 \pm 1.3$ | $-480 \pm 11$ | 0.42 | – | – | 0.16 |
| Summer | 1705 | $26.5 \pm 0.9$ | $-397 \pm 8$ | 0.35 | – | – | 0.15 |

Our data indicate that while local temperature is a key driver of autumn–winter seasonal variations of $\delta$D, which is consistent with temperature-driven distillation effects, this is not the case for spring–summer. During these seasons, the data depict a persistent but weaker relationship with logarithm of humidity (accounting for about 30 % of the variance), and a minor impact of temperature. We conclude that in spring–summer local processes controlling local humidity variations are independent of surface temperature and may be related to continental recycling and local evapotranspiration (Welp et al., 2012; Berkelhammer et al., 2013), or convective activity.

### 4.3 Diurnal variations

The period from May to September is characterised by the frequent occurrence of days with a strong diurnal d-excess cycle, which is not seen during other seasons (Fig. 6). This diurnal variability arises from small variations in humidity (1000–3000 ppmv) and $\delta^{18}$O (1–5 ‰), but with no counterpart in $\delta$D. This diurnal decoupling between $\delta$D and $\delta^{18}$O contrasts with the overall strong correlation depicted at the daily to seasonal scale (Fig. 7).

Following the analysis of Berkelhammer et al. (2013), we have performed an objective cluster analysis to characterise dominant diurnal cycle patterns. SciPy k-means clustering

routines have been used (Jones et al., 2001). The k-means clustering algorithm is one of the most used methods for vector quantisation. It is an iterative procedure, which partitions $n$ observations into $k$ clusters trying to minimise the sum of the squared distances between each observation and corresponding cluster. The starting centroids for each of the clusters are randomly chosen. At each iteration the centre of mass is recomputed for each cluster obtained in the previous step and observations are redistributed between the clusters in accordance with which of the new centre is nearer.

For the clustering analysis we have used only diurnal cycles, which are more than two-thirds complete. We focus on the period 8 May 2013 to 31 August 2013 giving us 104 nearby complete diurnal cycles. The data have been averaged on the 15 min basis. We chose not to normalise or detrend the data and varied the number of clusters. However, we did not obtained significant difference between the clusters when we tried to partition the cycles into more than two clusters. Whereas for the two-clusters calculation, the difference between the minimum d-excess values of the clusters (15 ‰) was 2.9 times larger than the standard deviation of the clusters. We have also performed an analysis of the meteorological conditions associated with each cluster. Here, we present the dominant patterns for d-excess, humidity and wind speed only and refer the reader to the Supplement for temperature, relative humidity, pressure and wind direction.

Figure 9 shows the dominant clusters for d-excess, humidity and wind speed. The red line (Cluster 1, 47 cycles) and the blue line (Cluster 2, 57 cycles) indicate the mean values of each cluster, with corresponding standard deviations shown by shading. The yellow bars show the time of sunrise (changing between 05:12 LT, on 8 May and 07:05 LT on 31 August) and similarly the dark red bars show sunset (changing between 21:07 LT on 8 May and 23:03 LT on 31 August). These two clusters show similar variability during the day, but differ by the magnitude of the d-excess night depletion (decrease of 21 ‰ and 7 ‰, respectively), related to the magnitude of the daily humidity peak level (increase of 2400 ppmv and 1000 ppmv, respectively) and the night mean wind speed (0.27 m s$^{-1}$ and 0.78 m s$^{-1}$, respectively).

The observed diurnal d-excess variability is similar to that reported by Berkelhammer et al. (2013), albeit they seem to only observe clusters similar to Cluster 1 (red line) and not Cluster 2 (blue line). This difference can be explained by the fact that the measurements of Berkelhammer et al. were carried out inside a mature open canopy (LAI = 1.9) ponderosa pine forest, while our measurements are carried out in a clearing of size $100 \times 100$ metres within the dense forest. We suggest that this allows turbulent night mixing to strongly reduce or even mask the diurnal cycle of d-excess caused by transpiration and dew formation. Within all the diurnal cycles, we observe an inverse correlation ($R = -0.74$, Fig. 10a) between the night mean wind speed (between 23:00 LT and 07:00 LT) and the magnitude of d-excess drop (difference between d-excess mean value for the interval from 15:00 LT to
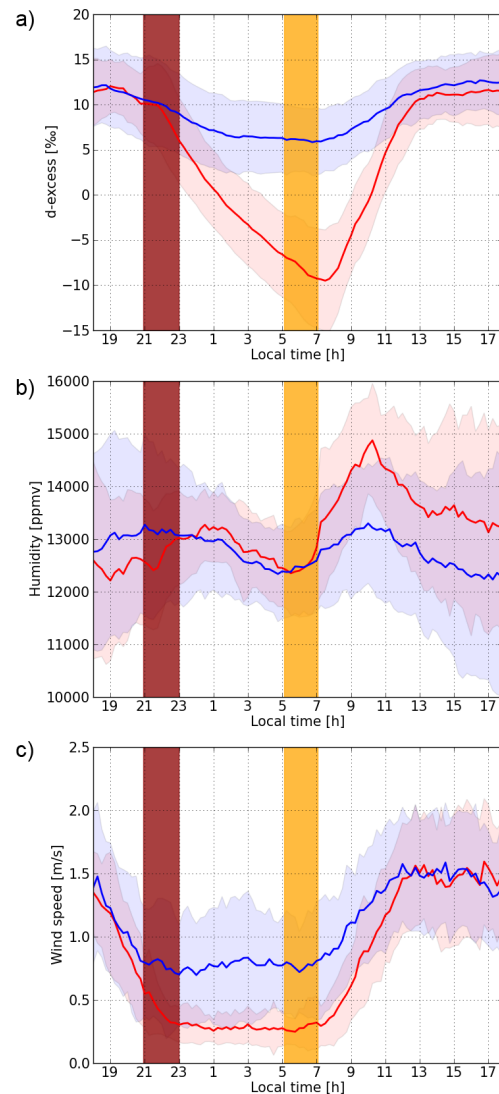


**Figure 9.** Dominant clusters for **(a)** d-excess, **(b)** humidity and **(c)** wind speed. Red line: Cluster 1, blue line: Cluster 2, yellow bars: sunrise time, dark red bars: sunset time. The shading shows the standard deviation for each cluster.

18:00 LT and mean value for the interval from 07:00 LT to 08:00 LT).

Similar d-excess diurnal cycles had also been reported by Welp et al. (2012) in the meta-analysis of water vapour measurements from six different sites located in various ecosystems (forest, grassland, agricultural and urban settings), all of which showed the general feature of d-excess midday increase with remarkably similar phases in the time progression. Throughout all the studies mentioned, the magnitude of d-excess daily variations ranges from $\sim 5$ ‰ to $\sim 20$ ‰ from site to site, but all share the same timing (decrease during the evening and the night with more rapid recovery in the morning).
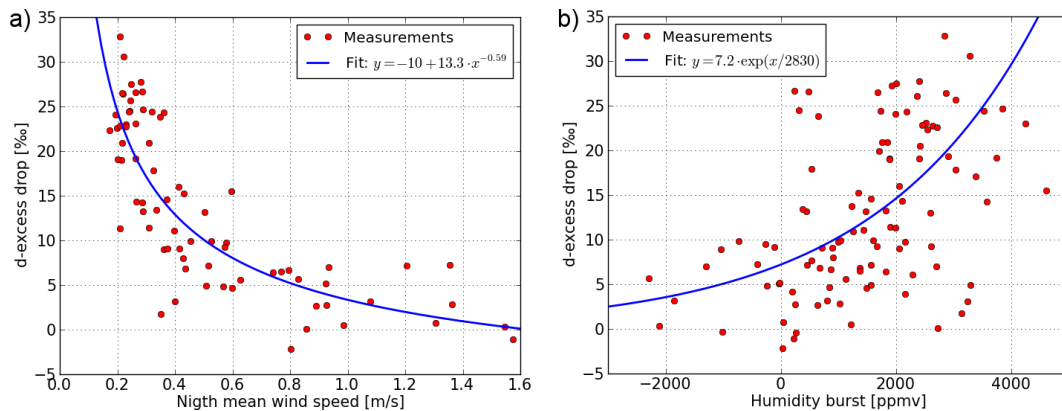
**Figure 10.** Deuterium excess drop vs. **(a)** night mean wind speed and **(b)** morning humidity burst.

Within all the diurnal cycles, we observe a positive correlation ($R = 0.49$, Fig. 10b) between the magnitude of d-excess drop and the humidity value increase during the morning burst (difference between humidity mean value for the interval from 09:30 LT to 10:30 LT and mean value for the interval from 05:00 LT to 06:00 LT). This finding is consistent with the mechanism proposed by Berkelhammer et al. (2013) whereby the diurnal d-excess cycle is a result of dew-fall and vapour-liquid interaction within the canopy. The morning burst is caused by initiation of transpiration and one would therefore expect (as our data also show) a positive correlation between the magnitude of d-excess drop and release of humidity in the morning.

## 5 Conclusions and perspectives

This study reports the successful use of a Picarro Inc. water vapour WS-CRDS analyzer for atmospheric water vapour isotope measurements at the surface in western Siberia (Kourovka, Russia). The measurement system and calibration protocol had been specifically adapted for the reliable performance at low humidity levels. Overall, the instrument demonstrated its ability to produce reliable measurements with an overall drift of less than 2 ‰ and 0.5 ‰ for $\delta$D and $\delta^{18}$O, respectively. Frequent calibrations reveal a good reproducibility with standard deviations of 0.9 ‰ and 0.25 ‰ for $\delta$D and $\delta^{18}$O, respectively.

At low humidity concentrations the measurements are subject to large errors. In particular, the Picarro standards delivery module requires further optimisation if it is to give reasonable calibration results for humidity levels below 4000 ppmv. We demonstrate that using dry air instead of DRIERITE produces excellent reproducibility for the isotope–humidity calibration curve established when using different standards.

During the monitoring campaign the isotopic composition varies in the range from −100 ‰ to −300 ‰ for $\delta$D, from −15 ‰ to −40 ‰ for $\delta^{18}$O and from +25 ‰ to −25 ‰ for d-excess with the humidity concentration being in the range

250–23 000 ppmv. The data set reveals considerable seasonal variations of isotopic composition and humidity concentration with a strong dependency on weather conditions. The strongest links are observed between $\delta$D and logarithm of humidity, and with temperature. However, these relationships are much weaker in spring–summer, especially for temperature.

The summer period shows a strong diurnal variability of d-excess, which was not seen during other seasons. This variability has a distinct relationship with sunset and sunrise and is consistent with interactions of dew-fall and canopy liquids with the atmospheric water vapour isotopes. During the night-time, d-excess experiences a strong decrease to negative values with the minimum occurring close to sunrise, after which it returns to the value affected by synoptic variability. By means of objective cluster analysis, two dominant patterns for d-excess are distinguished and associated patterns for meteorological parameters are determined. An inverse correlation is observed between the magnitude of d-excess diurnal decrease and the night wind speed and a positive correlation with the morning release of humidity.

The data obtained in this study provide a firm basis for further research of the atmospheric hydrological cycle of western Siberia. They are now available for comparison with remote-sensing measurements, outputs from moisture trajectory calculations, simulations of water vapour isotopic composition from land surface and boundary-layer models, or atmospheric general circulation models.

The work is part of a project investigating the water and carbon cycles in the permafrost and pristine peatlands of western Siberia and their projected changes under global warming. The full data set of isotopic and meteorological measurements discussed in this paper is available on the official site of the project WSibIso ("Impact of climate change on water and carbon cycles of melting permafrost of western Siberia"): http://www.wsibiso.ru, and in the web database of water isotope monitoring data: http://waterisotopes.lsce.ipsl.fr.

## References

Aemisegger, F., Sturm, P., Graf, P., Sodemann, H., Pfahl, S., Knohl, A., and Wernli, H.: Measuring variations of $\delta_{18}O$ and $\delta_2H$ in atmospheric water vapour using two commercial laser-based spectrometers: an instrument characterisation study, Atmos. Meas. Tech., 5, 1491–1511, doi:10.5194/amt-5-1491-2012, 2012.

Aemisegger, F., Pfahl, S., Sodemann, H., Lehner, I., Seneviratne, S. I., and Wernli, H.: Deuterium excess as a proxy for continental moisture recycling and plant transpiration, Atmos. Chem. Phys., 14, 4029–4054, doi:10.5194/acp-14-4029-2014, 2014.

Baer, D. S., Paul, J. B., Gupta, M., and O'Keefe, A.: Sensitive absorption measurements in the near-infrared region using off-axis integrated-cavity output spectroscopy, Appl. Phys. B-Lasers O., 75, 261–265, 2002.

Barkan, E. and Luz, B.: Diffusivity fractionations of $H_2^{16}O/H_2^{17}O$ and $H_2^{16}O/H_2^{18}O$ in air and their implications for isotope hydrology, Rapid Commun. Mass Sp., 21, 2999–3005, doi:10.1002/rcm.3180, 2007.

Berkelhammer, M., Hu, J., Bailey, A., Noone, D. C., Still, C. J., Barnard, H., Gochis, D., Hsiao, G. S., Rahn, T., and Turnipseed, A.: The nocturnal water cycle in an open-canopy forest, J. Geophys. Res.-Atmos., 118, 10225–10242, doi:10.1002/jgrd.50701, 2013.

Bonne, J.-L., Masson-Delmotte, V., Cattani, O., Delmotte, M., Risi, C., Sodemann, H., and Steen-Larsen, H. C.: The isotopic composition of water vapour and precipitation in Ivittuut, southern Greenland, Atmos. Chem. Phys., 14, 4419–4439, doi:10.5194/acp-14-4419-2014, 2014.

Brand, W. A., Geilmann, H., Crosson, E. R., and Rella, C. W.: Cavity ring-down spectroscopy versus high-temperature conversion isotope ratio mass spectrometry; a case study on $\delta^2H$ and $\delta^{18}O$ of pure water samples and alcohol/water mixtures, Rapid Commun. Mass Sp., 23, 1879–1884, doi:10.1002/rcm.4083, 2009.

Butzin, M., Werner, M., Masson-Delmotte, V., Risi, C., Frankenberg, C., Gribanov, K., Jouzel, J., and Zakharov, V. I.: Variations of oxygen-18 in West Siberian precipitation during the last 50 yr, Atmos. Chem. Phys. Discuss., 13, 29263–29301, doi:10.5194/acpd-13-29263-2013, 2013.

Ciais, P. and Jouzel, J.: Deuterium and oxygen 18 in precipitation: isotopic model, including mixed cloud processes, J. Geophys. Res.-Atmos., 99, 16793–16803, 1994.

Craig, H.: Standard for reporting concentrations of deuterium and oxygen-18 in natural waters, Science, 133, 1833–1834, 1961.

Craig, H. and Gordon, L.: Deuterium and oxygen-18 variations in the ocean and marine atmosphere, in: Stable Isotopes in Oceanography Studies and Paleotemperatures, 26–30 July 1965, Spoleto, Italy, 1965.

Crosson, E. R., Ricci, K. N., Richman, B. A., Chilese, F. C., Owano, T. G., Provencal, R. A., Todd, M. W., Glasser, J., Kachanov, A. A., Paldus, B. A., Spence, T. G., and Zare, R. N.: Stable isotope ratios using cavity ring-down spectroscopy: Determination of $^{13}C/^{12}C$ for carbon dioxide in human breath, Anal. Chem., 74, 2003–2007, doi:10.1021/ac025511d, 2002.

Dansgaard, W.: Stable isotopes in precipitation, Tellus, 16, 436–468, doi:10.1111/j.2153-3490.1964.tb00181.x, 1964.

Ellehoj, M. D., Steen-Larsen, H. C., Johnsen, S. J., and Madsen, M. B.: Ice-vapor equilibrium fractionation factor of hydrogen and oxygen isotopes: experimental investigations and implications for stable water isotope studies, Rapid Commun. Mass Sp., 27, 2149–2158, doi:10.1002/rcm.6668, 2013.

Farlin, J., Lai, C.-T., and Yoshimura, K.: Influence of synoptic weather events on the isotopic composition of atmospheric moisture in a coastal city of the western United States, Water Resour. Res., 49, 3685–3696, doi:10.1002/wrcr.20305, 2013.

Farquhar, G. D., Cernusak, L. A., and Barnes, B.: Heavy water fractionation during transpiration, Plant Physiol., 143, 11–18, 2007.

Field, R. D., Jones, D. B. A., and Brown, D. P.: Effects of postcondensation exchange on the isotopic composition of water in the atmosphere, J. Geophys. Res.-Atmos., 115, D24305, doi:10.1029/2010JD014334, 2010.

Galewsky, J., Rella, C., Sharp, Z., Samuels, K., and Ward, D.: Surface measurements of upper tropospheric water vapor isotopic composition on the Chajnantor Plateau, Chile, Geophys. Res. Lett., 38, L17803, doi:10.1029/2011GL048557, 2011.

Gat, J. R.: Oxygen and hydrogen isotopes in the hydrological cycle, Annu. Rev. Earth Pl. Sc., 24, 225–262, 1996.

Gonfiantini, R.: Standards for stable isotope measurements in natural compounds, Nature, 271, 534–536, 1978.

Gribanov, K., Jouzel, J., Bastrikov, V., Bonne, J.-L., Breon, F.-M., Butzin, M., Cattani, O., Masson-Delmotte, V., Rokotyan, N., Werner, M., and Zakharov, V.: ECHAM5-wiso water vapour isotopologues simulation and its comparison with WS-CRDS measurements and retrievals from GOSAT and ground-based FTIR spectra in the atmosphere of Western Siberia, Atmos. Chem. Phys. Discuss., 13, 2599–2640, doi:10.5194/acpd-13-2599-2013, 2013.

Gryazin, V., Risi, C., Jouzel, J., Kurita, N., Worden, J., Frankenberg, C., Bastrikov, V., Gribanov, K., and Stukova, O.: The added value of water isotopic measurements for understanding model biases in simulating the water cycle over Western Siberia, Atmos. Chem. Phys. Discuss., 14, 4457–4503, doi:10.5194/acpd-14-4457-2014, 2014.

Gupta, P., Noone, D., Galewsky, J., Sweeney, C., and Vaughn, B. H.: Demonstration of high-precision continuous measurements of water vapor isotopologues in laboratory and remote field deploy-

ments using wavelength-scanned cavity ring-down spectroscopy (WS-CRDS) technology, Rapid. Commun. Mass. Sp., 23, 2534–2542, 2009.

Han, L.-F., Groening, M., Aggarwal, P., and Helliker, B. R.: Reliable determination of oxygen and hydrogen isotope ratios in atmospheric water vapour adsorbed on 3A molecular sieve, Rapid. Commun. Mass. Sp., 20, 3612–3618, doi:10.1002/rcm.2772, 2006.

IAEA: Final Report on Fourth interlaboratory comparison exercise for $\delta^2$H and $\delta^{18}$O analysis of water samples (WICO2011), International Atomic Energy Agency (IAEA), 2012.

Jacob, H. and Sonntag, C.: An 8-year record of the seasonal variation of $^2$H and $^{18}$O in atmospheric water vapour and precipitation at Heidelberg, Germany, Tellus B, 43, 291–300, 1991.

Jones, E., Oliphant, T., and Peterson, P. SciPy: Open source scientific tools for Python, available at: http://www.scipy.org/, 2001–2014.

Jouzel, J.: Isotopes in cloud physics: Multistep and multistage processes, The Terrestrial Environment B, edited by: Fritz, P. and Fontes, J. C., Vol. 2, Handbook of Environmental Isotopes Geochemistry, Elsevier, 61–112, 1986.

Kerstel, E. R. T. and Gianfrani, L.: Advances in laser-based isotope ratio measurements: selected applications, Appl. Phys. B-Lasers O., 92, 439–449, 2008.

Kerstel, E. R. T., van Trigt, R., Dam, N., Reuss, J., and Meijer, H. A. J.: Simultaneous determination of the $^2$H/$^1$H, $^{17}$O/$^{16}$O, and $^{18}$O/$^{16}$O isotope abundance ratios in water by means of laser spectrometry, Anal. Chem., 71, 5297–5303, 1999.

Kurita, N.: Origin of Arctic water vapor during the ice-growth season, Geophys. Res. Lett., 38, L02709, doi:10.1029/2010GL046064, 2011.

Kurita, N., Newman, B. D., Araguas-Araguas, L. J., and Aggarwal, P.: Evaluation of continuous water vapor $\delta$D and $\delta^{18}$O measurements by off-axis integrated cavity output spectroscopy, Atmos. Meas. Tech., 5, 2069–2080, doi:10.5194/amt-5-2069-2012, 2012.

Kurita, N., Fujiyoshi, Y., Wada, R., Nakayama, T., Matsumi, Y., Hiyama, T. and Muramoto, K.: Isotopic variations associated with North-South displacement of the Baiu front, SOLA, 9, 187–190, 2013.

Kurita, N., Yoshida, N., Inoue, G., and Chayanova, E. A.: Modern isotope climatology of Russia: a first assessment, J. Geophys. Res.-Atmos., 109, D03102, doi:10.1029/2003JD003404, 2004.

Majoube, M.: Fractionnement en oxygène 18 et en deutérium entre l'eau et sa vapeur, J. Chim. Phys., 68, 1423–1436, 1971.

Merlivat, L.: Molecular diffusivities of H$_2^{16}$O, HD$^{16}$O and H$_2^{18}$O in gases, J. Chem. Phys., 69, 2864–2871, 1978.

Merlivat, L. and Jouzel, J.: Global climatic interpretation of the deuterium-oxygen 18 relationship for precipitation, J. Geophys. Res.-Oceans, 84, 5029–5033, doi:10.1029/JC084iC08p05029, 1979.

Merlivat, L. and Nief, G.: Fractionnement isotopique lors des changements d'état solide-vapeur et liquide-vapeur de l'eau à des températures inférieures à 0°C, Tellus, 19, 122–127, doi:10.1111/j.2153-3490.1967.tb01465.x, 1967.

Rozanski, K., Araguás-Araguás, L., and Gonfiantini, R.: Isotopic patterns in modern global precipitation, in: Geophraphical Monograph Series, edited by: Swart, P. K., Lohmann, K. C., McKenzie, J., and Savin, S., Vol. 78, American Geophysical Union, Washington DC, 1–36, 1993.

Shalaumova, Y. V., Fomin, V. V., and Kapralov, D. S.: Spatiotemporal dynamics of the Urals climate in the second half of the 20th century, Russ. Meteorol. Hydrol., 35, 107–114, 2010.

Steen-Larsen, H. C., Johnsen, S. J., Masson-Delmotte, V., Stenni, B., Risi, C., Sodemann, H., Balslev-Clausen, D., Blunier, T., Dahl-Jensen, D., Ellehøj, M. D., Falourd, S., Grindsted, A., Gkinis, V., Jouzel, J., Popp, T., Sheldon, S., Simonsen, S. B., Sjolte, J., Steffensen, J. P., Sperlich, P., Sveinbjörnsdóttir, A. E., Vinther, B. M., and White, J. W. C.: Continuous monitoring of summer surface water vapor isotopic composition above the Greenland Ice Sheet, Atmos. Chem. Phys., 13, 4815–4828, doi:10.5194/acp-13-4815-2013, 2013.

Steen-Larsen, H. C., Masson-Delmotte, V., Hirabayashi, M., Winkler, R., Satow, K., Prié, F., Bayou, N., Brun, E., Cuffey, K. M., Dahl-Jensen, D., Dumont, M., Guillevic, M., Kipfstuhl, S., Landais, A., Popp, T., Risi, C., Steffen, K., Stenni, B., and Sveinbjörnsdottír, A. E.: What controls the isotopic composition of Greenland surface snow?, Clim. Past, 10, 377–392, doi:10.5194/cp-10-377-2014, 2014.

Stewart, M. K.: Stable isotope fractionation due to evaporation and isotopic exchanges of falling water drops: applications to atmospheric processes and evaporation of lakes, J. Geophys. Res., 80, 1133–1146, 1975.

Strong, M. Z. D., Sharp, D., and Gutzler, D. S.: Diagnosing moisture transport using D/H ratios of water vapor, Geophys. Res. Lett., 34, L03404, doi:10.1029/2006GL028307, 2007.

Sturm, P. and Knohl, A.: Water vapor $\delta_2$H and $\delta_{18}$O measurements using off-axis integrated cavity output spectroscopy, Atmos. Meas. Tech., 3, 67–77, doi:10.5194/amt-3-67-2010, 2010.

Tremoy, G., Vimeux, F., Cattani, O., Mayaki, S., Souley, I., and Favreau, G.: Measurements of water vapor isotope ratios with wavelength-scanned cavity ring-down spectroscopy technology: new insights and important caveats for deuterium excess measurements in tropical areas in comparison with isotope-ratio mass spectrometry, Rapid Commun. Mass Sp., 25, 3469–3480, doi:10.1002/rcm.5252, 2011.

Tremoy, G., Vimeux, F., Mayaki, S., Souley, I., Cattani, O., Risi, C., Favreau, G., and Oi, M.: A 1-year long $^{18}$O record of water vapor in Niamey (Niger) reveals insightful atmospheric processes at different timescales, Geophys. Res. Lett., 39, L08805, doi:10.1029/2012GL051298, 2012.

Uemura, R., Matsui, Y., Yoshimura, K., Motoyama, H., and Yoshida, N.: Evidence of deuterium excess in water vapor as an indicator of ocean surface conditions, J. Geophys. Res.-Atmos., 113, D19114, doi:10.1029/2008JD010209, 2008.

Welp, L. R., Lee, X., Griffis, T. J., Wen, X.-F., Xiao, W., Li, S., Sun, X., Hu, Z., Martin, M. V., and Huang, J.: A meta-analysis of water vapor deuterium-excess in the midlatitude atmospheric surface layer, Global Biogeochem. Cy., 26, GB3021, doi:10.1029/2011GB004246, 2012.

Wen, X.-F., Zhang, S.-C., Sun, X.-M., Yu, G.-R., and Lee, X.: Water vapor and precipitation isotope ratios in Beijing, China, J. Geophys. Res., 115, doi:10.1029/2009JD012408, 2011.